**Supplementary Note 1**

**Flagella isolation**

Flagella were isolated following a modified version of a published protocol[57]. Briefly, cells were harvested at 22°C for 2 min at 10,000 × g and washed with 10 mM HEPES (pH 7.4). 5% (w/v) sucrose solution was added to the cells prior to pH shock. 0.5 M acetic acid was added to the sample until the pH reached 4.5. The pH was monitored by using a pH meter. The sample was kept at pH 4.5 for 1 minute and then was quickly neutralized to pH 7.0 by addition of 0.5 M NaOH. After pH shock, the cells were centrifuged at 22°C for 5 min at 2,000 × g to remove cell bodies. The supernatant, which contains the flagella, was collected and loaded onto a 25% sucrose cushion (10 mM HEPES, pH 7.4, 5 mM $MgSO_4$, 1 mM DTT, 25% sucrose) and centrifuged at 4°C for 10 min at 2,500 × g. The flagella-containing supernatant was collected down to the sucrose interface and centrifuged at 4°C for 20 min at 10,000 × g to pellet the flagella. The pellets were resuspended with a buffer containing 30 mM HEPES, pH 7.4, 5 mM $MgSO_4$, 1 mM DTT, 0.5 mM EGTA, 50 mM KCl and 1x protease inhibitor cocktail (Roche). The purified flagella were either directly used for radial spoke purification or stored at -80 °C for future use.

**Radial spoke purification**

All purification steps were conducted on ice or at 4°C. To solubilize the flagella membrane, NP-40 detergent solution (Thermo Fisher Scientific) was added to purified flagella to a final concentration of 0.5 % (w/v) and incubated for 30 min before centrifuging at 15,000 × g for 30 min. The pellet, which contains the axoneme, was resuspended with HMDEK buffer (20 mM HEPES, pH 7.4, 5 mM $MgSO_4$, 1 mM DTT, 1 mM EGTA, 50 mM KCl) containing 1x ProteaseArrest protease inhibitors (G-Biosciences). To remove dynein arms, a final concentration of 1 mM ATP and 0.5 M NaCl was added to the resuspended axonemes and incubated for 30 min before centrifuging at 15,000 × g for 30 min. The pellets were resuspended with HMDEK buffer containing 1x ProteaseArrest protease inhibitors. To extract radial spokes from the doublet microtubules, a final concentration of 0.6 M NaI was added and incubated for 30 min before centrifuging at 15,000 × g for 30 min. After centrifugation, the supernatant, which contains the radial spokes, was concentrated and exchanged to HMDEK buffer without NaI by spin

centrifugation using a 100-kDa cut-off concentrator (Thermo Fisher Scientific). The final volume of the sample was ~0.5 mL.

The extracted radial spokes (0.5 mL volume) were loaded onto a 10–25% continuous sucrose gradient in HMDEK buffer containing 1x ProteaseArrest protease inhibitors. The volume of the sucrose gradient was ~11.5 mL, made using a Gradient Master (BioComp Instruments, Inc.). Centrifugation was performed at 36,000 rpm (221,633 x g, SW41 rotor, Beckman Coulter) for 16 h with max acceleration and no braking. The resulting gradients were fractionated by hand into 21 equal fractions (600 mL each fraction). Fractions 14 to 20 (from top to bottom) were collected and loaded onto a monoQ 5/50 GL anion-exchange column (GE Healthcare) pre-equilibrated with HMDE buffer (20 mM HEPES, pH 7.4, 5 mM $MgSO_4$, 1 mM DTT, 1 mM EGTA) and eluted with a 0–1 M KCl gradient in HMDE buffer. The radial spokes eluted at ~0.7 M KCl. The high salt concentration needed to elute radial spokes from the anion-exchange column possible reflects the highly electronegatively charged surface of the radial spokehead (Fig. 3c). The eluted fractions were concentrated and exchanged to HMDE buffer with 150 mM KCl by spin centrifugation using a 100-kDa cut-off concentrator (Thermo Fisher Scientific) for electron microscopy studies. For one purification, we typically started with 64 L cells and obtained ~35 uL purified radial spokes at a concentration between 0.50 mg/mL to 0.75 mg/mL.

SDS-PAGE were performed for the sucrose gradient fractions and the monoQ elution and the gels were stained with a silver stain kit (Thermo Fisher Scientific).

**Model Building Strategies**

*1. Manual fold recognition*. Homology models for each RSP were generated using SWISS-MODEL[80] and I-TASSER[81]. Reasonable models for RSP4, RSP5, RSP6, RSP12, RSP16 and LC8 could be built based on templates identified from the Protein Databank (PDB). Visual inspection of the cryo-EM map was sufficient to identify where these homology models should be placed. The models were then modified in Coot[68] to better fit the density. This strategy also identified

an armadillo fold in the stalks of both radial spokes, with sidechain density used to distinguish between RSP14 in RS1 and RS8 in RS2.

*2. Automated density-guided fold recognition*. Density that corresponded to globular domains that could not be assigned by manual inspection, were cut from the map and compared with a library of protein domains using the MOLREP-BALBES pipeline for density-guided fold recognition[82]. This strategy was used to identify actin in IDA*c*. Density for actin was initially divided into two halves. The top hit for the first half was subdomains 1 and 2 of monomeric actin (PDB 2HF3, contrast score = 10.9). The top hit for the second half was subdomains 3 and 4 of actin (PDB 3MN5, contrast score = 8.8). Additional density is observed in a deep cleft between domains 1/2 and 3/4 that could correspond to either ADP or ATP. Automated density-guided fold recognition also identified two ubiquitin-like domains in the radial spoke stalks: one in the neck (PDB 1EF1, contrast score = 8.3) and one near the base of RS2 (PDB 3L0W, contrast score = 5.7). The ubiquitin-like domain in the neck could be assigned to FAP198 based on sidechain density, but the identity of the ubiquitin-like domain at the base of RS2 remains unknown. Once the identity of FAP198 was known, its N-terminal cytochrome b5 domain was modeled based on a homology model.

*3. Secondary structure profile*. Once proteins with identified folds had been placed, idealized secondary structure elements were built into the remaining density using Coot. The length and connectivity of these secondary structure elements were compared to secondary structure profiles predicted by JPred4[83] or PSIPRED[84] of all proteins identified in the samples by mass spectrometry. This strategy assigned the radial-spoke-spanning $\alpha$-helices to RSP3 and three proteins containing repetitive $\beta$-strands to RSP1, RSP10, and FAP207. The proteins were distinguished based on sidechain density.

We also observed clear density in the RS2 stalk that corresponded to the alternating $\alpha$-helices and $\beta$-strands pattern of leucine-rich-repeat containing proteins. Comparison with the predicted secondary structure profiles identified FAP201-like (Phytozome gene Cre09.g397993)

as being the mostly likely protein. This assignment was confirmed by the sidechain density. The sequence of FAP201-like matches a single 50-residue peptide obtained by mass spectrometry analysis of RSP15[49], allowing us to conclude that FAP201-like is the previously unassigned RSP15.

*4. De novo sequence assignment*. Many RSPs have little to no known homology with proteins with determined structures and therefore could not be identified by fold recognition or secondary structure assignment. These proteins (RSP9, FAP91 and FAP253) were identified by assigning sequence, based on sidechain density, to poly(alanine) models built *de novo* in Coot.

We also identified three subunits of the N-DRC (DRC1, DRC2, and DRC4) using *de novo* sequence assignment. This was not possible with the lower-resolution maps that we reported previously[21]. Our assignment of the N-DRC subunits is consistent with subtomogram averages of *Chlamydomonas* axonemes isolated from strains with specific DRC subunit deletions or rescued strains with tagged DRC subunits[85].

*5. Prior knowledge.* Previous work had shown that RSP3 binds proteins with RIIa or Dpy-30 domains[38,86,87]. We therefore visually scanned RSP3 for interactions resembling the AKAP:RIIa complex structure (PDB 4ZP3)[88]. The first interaction we identified were the RIIa motifs of the RSP7/RSP11 heterodimer followed by the Dpy-30 motifs of RSP2/RSP23 and RSP4/RSP6. These different heterodimers are distinguishable based on sidechain density.

Additional density consistent with a homodimer with long $\alpha$-helices was observed in the map for IDA*c*. This homodimer could be assigned to p28 based on i) p28 being a known component of IDA*c*[39], ii) reports that p28 is a homodimer[41], iii) a reported interaction between p28 and actin[41], and iv) the presence of long $\alpha$-helices in its secondary structure profile.

*6. Bioinformatic identification.* Extra density could be observed bound to a long helix of FAP253 at the base of RS1. This helix was predicted to contain a calmodulin-binding IQ motif by

SMART[89]. Guided by this prediction, a homology model of *Chlamydomonas* calmodulin was built using SWISS-MODEL[80] and fitted to the density. Comparison with structures of calmodulin bound to the IQ motif of myosin in apo- and $Ca^{2+}$-bound states[42,43], revealed the density in RS1 is consistent with apo-calmodulin. Bioinformatic identification by SMART was also used to identify a Dpy-30 motif in FAP385 and assign it to density corresponding to an orphan Dpy-30 domain in the neck.

## Supplementary Tables

## Supplementary Table 1 | Identified proteins in the density maps.

| Proteins | Phytozome v5 gene* | UniProt / NCBI accession numbers | Mass (kDa) | Length (residues) | Protein identification method | Model accuracy | Built residues‡ |
|---|---|---|---|---|---|---|---|
| RSP1 | Cre03.g201900 | Q27YU0 / XP_001693353.1 | 87.8 | 814 | Secondary structure profile | Sidechain | 14-256, 261-302, 343-751, 760-814 |
| RSP2 | Cre10.g427300 | Q6UBQ3 / XP_001702718.1 | 77.4 | 738 | Fold recognition, *de novo* assignment | Sidechain | 8-127, 233-362, 434-610 |
| RSP3 | Cre06.g291700 | A8J2J7 / XP_001695406.1 | 56.8 | 516 | Secondary structure profile | Sidechain | 95-264, 268-386, 468-509 |
| RSP4 | Cre05.g242500 | A8I550 / XP_001700728.1 | 49.8 | 465 | Fold recognition | Sidechain | 6-175, 203-453 |
| RSP5 | Cre12.g544000 | - / XP_001694084.1 | 49.3 | 521 | Fold recognition | Sidechain | 16-63, 78-316, 323-518 |
| RSP6 | Cre05.g242550 | A8I554 / XP_001700729.1 | 48.8 | 459 | Fold recognition | Sidechain | 4-319, 330-430, 439-449 |
| RSP7 | Cre07.g347050 | - / PNW81221.1 | 54.7 | 500 | Fold recognition, *de novo* assignment | Sidechain | 1-47 |
| RSP8 | Cre02.g078600 | Q27YU6 / XP_001701869.1 | 40.5 | 378 | Fold recognition | Fold | 41-347 |
| RSP9 | Cre07.g330200 | Q27YU5 / XP_001690441.1 | 29.5 | 269 | *De novo* assignment | Sidechain | 2-123, 143-269 |
| RSP10 | Cre01.g005450 | Q27YU4 / XP_001702125.1 | 23.5 | 216 | Secondary structure profile | Sidechain | 8-33, 43-215 |
| RSP11 | Cre10.g465250 | Q27YU3 / XP_001698630.1 | 21.5 | 204 | Fold recognition, *de novo* assignment | Sidechain (1-54). Fold. | 1-90, 94-108, 114-201 |
| RSP12 | Cre02.g114700 | A8I2U9 / XP_001699890.1 | 19.6 | 181 | Fold recognition | Sidechain | 17-179 |
| RSP14 | Cre14.g617500 | A8HNV0 / XP_001690282.1 | 40.6 | 387 | Fold recognition, *de novo* assignment | Sidechain | 2-380 |
| RSP15† (FAP201-like) | Cre09.g397993 | A0A2K3DEQ5 / PNW79021 | 35.3 | 331 | Secondary structure profile | Sidechain | 5-331 |
| RSP16 | Cre12.g511050 | A8IKR9 / XP_001690875.1 | 39.0 | 346 | Fold recognition | Sidechain | 6-69, 134-346 |
| RSP20 (Calmodulin) | Cre03.g178150 | A8IDP6 / XP_001703420.1 | 18.3 | 163 | Bioinformatic identification | Fold | 8-150 |
| RSP22 (LC8) | Cre03.g181150 | A8JH45 / XP_001702907.1 | 10.3 | 91 | Fold recognition | Sidechain | 7-90 |
| RSP23 | Cre16.g654300 | Q69B19 / XP_001698136.1 | 61.4 | 586 | Fold recognition, *de novo* assignment | Sidechain | 4-204 |
| FAP91 (RSP18) | Cre07.g330700 | A8IH47 / XP_001690436.1 | 107.2 | 1029 | *De novo* assignment | Sidechain | 181-200, 213-234, 244-398, 414-440 |
| FAP198† | Cre09.g403200 | A0A2K3DCN8 / PNW78294.1 | 26.6 | 230 | Automated density-guided fold recognition | Sidechain | 10-175, 181-227 |
| FAP207 | Cre07.g328350 | A0A2K3DJP7 / PNW80755.1 | 28.4 | 256 | Secondary structure profile | Sidechain | 11-214 |
| FAP253† | Cre12.g502000 | A0A2K3D359 / PNW74974.1 | 74.9 | 682 | *De novo* assignment | Sidechain (358-394, | 344-394, 398-539, |

| | | | | | | | |
|---|---|---|---|---|---|---|---|
| | | | | | | 461-539, 554-650). Fold. | 554-650 |
| FAP385† | Cre12.g495550 | A8JDM3 / XP_001700549.1 | 8.1 | 70 | Bioinformatic identification and fold recognition. | Sidechain | 17-66 |
| Actin | Cre13.g603700 | A8JAV1 / XP_001699068.1 | 41.8 | 377 | Automated density-guided fold recognition | Sidechain | 8-377 |
| p28 | - | Q39604 / XP_001700527.1 | 28.7 | 253 | Prior knowledge | Sidechain | 78-229 |
| DRC1 | - | P0DL09 / AFU81554.1 | 79.3 | 698 | *De novo* assignment | Sidechain | 330-413, 615-698 |
| DRC2 | Cre13.g607750 | A8JB22 / A8JB22.2 | 64.9 | 573 | *De novo* assignment | Sidechain | 277-374, 449-533 |
| DRC4 | Cre11.g476850 | Q7XJ96 / Q7XJ96.1 | 55.1 | 471 | *De novo* assignment | Sidechain | 294-466 |
| CCDC39 | Cre17.g701250 | A0A0A1H1F6 / PNW69992.1 | 105.3 | 925 | Prior knowledge | Sidechain | 31-260, 515-661, 673-730 |
| CCDC40 | Cre17.g698365 | A0A0A1GYE8 / BAP87096.1 | 101.2 | 904 | Prior knowledge | Sidechain | 29-264, 523-670, 677-727 |

*For each protein, accession numbers are reported for the Phytozome, UniProt, and NCBI databases. If an entry does not match the other two, the accession number is excluded and marked with a (-).

†Novel RSPs identified in this study.

‡Residues of RSP3, RSP11 and FAP253 were built using the composite maps of isolated RS1 (EMD-22475) and the on-doublet RS2 stalk (EMD-22481). For RSP11 and FAP253, residues with sidechain accuracy are listed and sidechains of the other residues are truncated due to the map quality.

## Supplementary Table 2 | Stoichiometries and locations of Radial Spoke Proteins (RSPs).

| Proteins | Copies in RS1 | Copies in RS2 | Location | Present in radial spoke precursor?[†] |
|---|---|---|---|---|
| RSP1 | 2 | 2 | Spokehead. | Yes |
| RSP2 | 2 | 2 | Spokehead. | Yes |
| RSP3 | 2 | 2 | Spans entire length. | Yes |
| RSP4 | 2 | 2 | Spokehead. | Yes |
| RSP5 | 2 | 2 | Spokehead. | Yes |
| RSP6 | 2 | 2 | Spokehead. | Yes |
| RSP7 | 2 | 2 | Stalk. | Yes |
| RSP8 | 0 | 1 | Stalk. RS2 specific. | No |
| RSP9 | 4 | 4 | Spokehead. | Yes |
| RSP10 | 2 | 2 | Spokehead. | Yes |
| RSP11 | 2 | 2 | Stalk. | Yes |
| RSP12 | 1 | 1 | Neck. | Yes |
| RSP14 | 1 | 0 | Stalk. RS1 specific. | Unknown |
| RSP15 | 0 | 1 | Stalk. RS2 specific. | Unknown |
| RSP16 | 2 | 2 | Neck and spokehead. | No |
| RSP20 (calmodulin)* | 1 | 0 | Stalk. | Unknown |
| RSP22 (LC8) | 8 | 12 | Stalk. | Unknown |
| RSP23 | 2 | 2 | Spokehead. | Unknown |
| FAP91 (RSP18) | 0 | 1 | Base of stalk. Binds doublets. RS2 specific. | Unknown |
| FAP198 | 1 | 1 | Neck. | Unknown |
| FAP207 | 1[‡] | 1 | Base of stalk. Binds doublets. | Unknown |
| FAP253 | 1 | 0 | Base of stalk. Binds doublets. RS1 specific. | Unknown |
| FAP385 | 2 | 2 | Neck. | Unknown |

*A calmodulin-binding IQ motif in a flexible and unobserved region of RSP23 suggests the total number of calmodulin molecules may be greater than identified.

[†]Based on observations reported in[28,34].

[‡]Due to the map quality of the on-doublet RS1 stalk we cannot unambiguously identify FAP207 at the base of RS1. Its assignment is based on similarity of the density with FAP207 in the RS2 stalk.

**Supplementary Table 3 | Relationship between identified proteins, motility defects in *Chlamydomonas* strains, and human disease including primary ciliary dyskinesia (PCD).**

| Protein | *Chlamydomonas* mutant strain | *Chlamydomonas* phenotype | Human ortholog (Uniprot ID) | Human disease association |
|---|---|---|---|---|
| RSP1 | | | RSPH1 (Q8WYR4) | PCD with central pair and radial-spoke defects[90]. |
| RSP2 | *pf24* | Paralyzed with loss of spokehead and neck[13,91,92]. | DYDC2 (Q96IM9) | - |
| RSP3 | *pf14* | Paralyzed with loss of radial spokes[11,13,17,49,93,94]. | RSPH3 (Q86UC2) | PCD with central pair and radial-spoke defects[95]. |
| RSP4 | *pf1* | Paralyzed with loss of spokehead[13,91,96]. | RSPH4A (Q5TD94) | PCD with central pair and radial-spoke defects[97]. |
| RSP5 | | | - | - |
| RSP6 | *pf26* | Impaired motility[91,98]. | RSPH6 (Q9H0K4) | *Rsph6a* knockout male mice are infertile with immotile spermatozoa[99]. |
| RSP7 | | | - | - |
| RSP8 | | | - | - |
| RSP9 | *pf17* | Paralyzed with loss of spokehead .[91]. | RSPH9 (Q9H1X1) | PCD with central pair and radial-spoke defects[97]. |
| RSP10 | | | RSPH10B (P0C881) | - |
| RSP11 | *pf25* | Spectrum of motility from paralysis to twitching to wild-type like swimming[49,91]. | RSPH11 (Q96C74) | - |
| RSP12 | | | PPIL6 (Q8IXY8) | - |
| RSP14 | | | RSPH14 (Q9UHP6) | - |
| RSP15 | | | LRRC34 (Q8IZ02) | - |
| RSP16 | *pf33* | Jerky motility with structural flexibility in spokehead and neck[29]. | DNAJB13 (P59910) | PCD with central pair defects[30]. |
| RSP20 | | | Calmodulin (P0DP23) | - |
| RSP22 | *fla14* | Paralyzed with loss of radial spokes[100,101]. | DYNLL1 (P63167) | - |
| RSP23 | *ndk5* | Paralyzed with short flagella. Radial spokes lack spokehead and neck[102]. | NME5 (P56597) | Down regulated in bronchial tissue of PCD patients[103]. |
| FAP91 | 4A2 (miRNA knockdown) | Reduced swim speed[24] with loss of RS2[104]. Occasional presence of an additional radial spoke located at irregular and variable intervals[104]. | CFAP91/MAATS1 (Q7Z4T9) | Male infertility with central pair and radial-spoke defects[105]. |
| FAP198 | | | CYB5D1 (Q6P9G0) | |
| FAP207 | | | MORN3 (Q6PF18) | Reported to regulate spermatogenesis[106]. |
| FAP253 | | | IQUB (Q8NA54) | IQUB mutants have elongated cilia[107]. |
| FAP385 | | | - | - |
| Actin | *ida5* | Slow swimming with loss of IDA *a, c, d, e*[108]. | Actin (P62736) | - |
| p28 | *ida4* | Slow swimming with loss of IDA *a, c, d*[13,109]. | DNALI1 (O14645) | - |
| DRC1 | *pf3* | Slow swimming[110]. | DRC1 (Q96MC2) | PCD[111]. |
| DRC2 | *pf5* | Slow swimming[110]. | DRC2 (Q8IXS2) | PCD[112]. |
| DRC4 | *pf2-4* | Slow swimming[113]. | DRC4 (O95995) | PCD[114]. |
| CCDC39 | *pf8* | Short flagella with axonemal organization defects[96]. | CCDC39 (Q9UFE4) | PCD with laterality abnormalities[115]. |
| CCDC40 | *pf9* | Short flagella with axonemal organization defects[96]. | CCDC40 (Q4G0X9) | PCD with laterality abnormalities[116]. |

**Supplementary Figure**

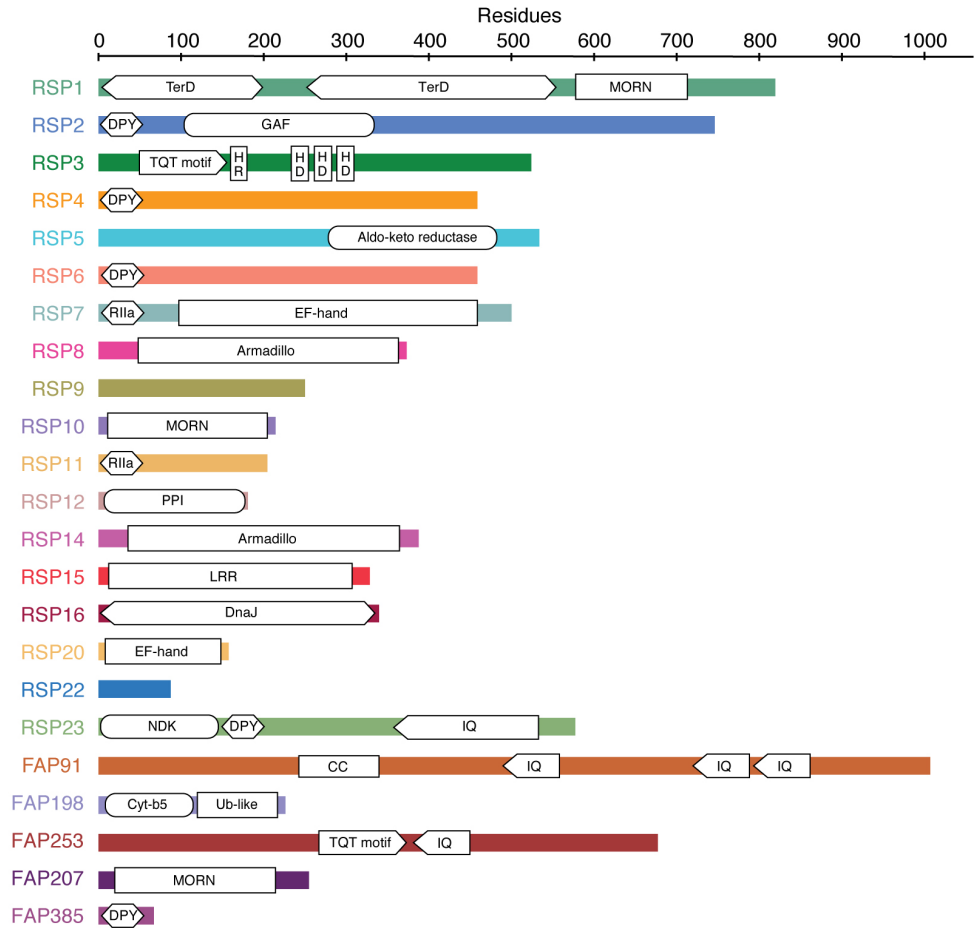


**Supplementary Fig. 1 | Domain architecture.**

Domain architecture of radial spoke proteins (RSPs) identified in the cryo-EM maps. Domains and domain boundaries were annotated from the atomic models or by using SMART[89] or Pfam[117] to analyze primary sequences. Abbreviations: TerD, TerD domain; MORN, Membrane Occupation and Recognition Nexus repeat; DPY, Dpy-30 motif; GAF, cyclic GMP-specific phosphodiesterases, adenylyl cyclase, FhlA domain; TQT motif, LC8-binding TQT motif; HR, RIIa-binding amphipathic helix; HD, Dpy-30-binding amphipathic helix; Aldo-keto reductase; RIIa, Regulatory subunit portion of type II protein kinase A regulatory subunit; EF-hand, helix-loop-helix typically associated with calcium binding; Armadillo, Armadillo repeat-containing domain; PPI, Cyclophilin-type peptidyl-prolyl cis-trans isomerase; DnaJ, DnaJ domain; NDK, Nucleoside diphosphate kinase; IQ, IQ calmodulin-binding motif; CC, coiled-coil; Cyt-b5, Cytochrome b5-like Heme/Steroid binding domain; Ub-like, ubiquitin-like domain.

**References**


80. Waterhouse, A. *et al.* SWISS-MODEL: homology modelling of protein structures and complexes. *Nucleic Acids Research* **46,** W296–W303 (2018).
81. Yang, J. *et al.* The I-TASSER Suite: protein structure and function prediction. *Nat. Methods* **12,** 7–8 (2015).
82. Brown, A. *et al.* Tools for macromolecular model building and refinement into electron cryo-microscopy reconstructions. *Acta Crystallogr. D Biol. Crystallogr.* **71,** 136–153 (2015).
83. Drozdetskiy, A., Cole, C., Procter, J. & Barton, G. J. JPred4: a protein secondary structure prediction server. *Nucleic Acids Research* **43,** W389–94 (2015).
84. Buchan, D. W. A. & Jones, D. T. The PSIPRED Protein Analysis Workbench: 20 years on. *Nucleic Acids Research* **47,** W402–W407 (2019).
85. Gui, L. *et al.* Scaffold subunits support associated subunit assembly in the Chlamydomonas ciliary nexin-dynein regulatory complex. *Proc. Natl. Acad. Sci. U.S.A.* **110,** 201910960 (2019).
86. Gopal, R., Foster, K. W. & Yang, P. The DPY-30 domain and its flanking sequence mediate the assembly and modulation of flagellar radial spoke complexes. *Molecular and Cellular Biology* **32,** 4012–4024 (2012).
87. Sivadas, P., Dienes, J. M., St Maurice, M., Meek, W. D. & Yang, P. A flagellar A-kinase anchoring protein with two amphipathic helices forms a structural scaffold in the radial spoke complex. *J. Cell Biol.* **199,** 639–651 (2012).
88. Götz, F. *et al.* AKAP18:PKA-RIIα structure reveals crucial anchor points for recognition of regulatory subunits of PKA. *Biochem. J.* **473,** 1881–1894 (2016).
89. Letunic, I. & Bork, P. 20 years of the SMART protein domain annotation resource. *Nucleic Acids Research* **46,** D493–D496 (2018).
90. Kott, E. *et al.* Loss-of-function mutations in RSPH1 cause primary ciliary dyskinesia with central-complex and radial-spoke defects. *Am. J. Hum. Genet.* **93,** 561–570 (2013).
91. Huang, B., Piperno, G., Ramanis, Z. & Luck, D. J. Radial spokes of Chlamydomonas flagella: genetic analysis of assembly and function. *J. Cell Biol.* **88,** 80–88 (1981).
92. Yang, P., Yang, C. & Sale, W. S. Flagellar radial spoke protein 2 is a calmodulin binding protein required for motility in Chlamydomonas reinhardtii. *Eukaryotic Cell* **3,** 72–81 (2004).
93. Witman, G. B., Plummer, J. & Sander, G. Chlamydomonas flagellar mutants lacking radial spokes and central tubules. Structure, composition, and function of specific axonemal components. *J. Cell Biol.* **76,** 729–747 (1978).
94. Diener, D. R., Ang, L. H. & Rosenbaum, J. L. Assembly of flagellar radial spoke proteins in Chlamydomonas: identification of the axoneme binding domain of radial spoke protein 3. *J. Cell Biol.* **123,** 183–190 (1993).
95. Jeanson, L. *et al.* RSPH3 Mutations Cause Primary Ciliary Dyskinesia with Central-Complex Defects and a Near Absence of Radial Spokes. *Am. J. Hum. Genet.* **97,** 153–162 (2015).
96. McVittie, A. Flagellum mutants of Chlamydomonas reinhardii. *J. Gen. Microbiol.* **71,** 525–540 (1972).

97. Castleman, V. H. *et al.* Mutations in radial spoke head protein genes RSPH9 and RSPH4A cause primary ciliary dyskinesia with central-microtubular-pair abnormalities. *Am. J. Hum. Genet.* **84,** 197–209 (2009).
98. Curry, A. M., Williams, B. D. & Rosenbaum, J. L. Sequence analysis reveals homology between two proteins of the flagellar radial spoke. *Molecular and Cellular Biology* **12,** 3967–3977 (1992).
99. Abbasi, F. *et al.* RSPH6A is required for sperm flagellum formation and male fertility in mice. *J. Cell. Sci.* **131,** jcs221648 (2018).
100. Pazour, G. J., Wilkerson, C. G. & Witman, G. B. A dynein light chain is essential for the retrograde particle movement of intraflagellar transport (IFT). *J. Cell Biol.* **141,** 979–992 (1998).
101. Yang, P., Yang, C., Wirschell, M. & Davis, S. Novel LC8 mutations have disparate effects on the assembly and stability of flagellar complexes. *J. Biol. Chem.* **284,** 31412–31421 (2009).
102. Zhu, X. *et al.* General and specific promotion of flagellar assembly by a flagellar nucleoside diphosphate kinase. *Mol. Biol. Cell* **28,** 3029–3042 (2017).
103. Geremek, M. *et al.* Ciliary genes are down-regulated in bronchial tissue of primary ciliary dyskinesia patients. *PLoS ONE* **9,** e88216 (2014).
104. Heuser, T., Dymek, E. E., Lin, J., Smith, E. F. & Nicastro, D. The CSC connects three major axonemal complexes involved in dynein regulation. *Mol. Biol. Cell* **23,** 3143–3155 (2012).
105. Martinez, G. *et al.* Biallelic variants in MAATS1 encoding CFAP91, a calmodulin-associated and spoke-associated complex protein, cause severe astheno-teratozoospermia and male infertility. *J. Med. Genet.* jmedgenet–2019–106775 (2020).
106. Zhang, L. *et al.* Characterization of membrane occupation and recognition nexus repeat containing 3, meiosis expressed gene 1 binding partner, in mouse male germ cells. *Asian J. Androl.* **17,** 86–93 (2015).
107. Lai, C. K. *et al.* Functional characterization of putative cilia genes by high-content analysis. *Mol. Biol. Cell* (2011).
108. Kato, T., Kagami, O., Yagi, T. & Kamiya, R. Isolation of two species of Chlamydomonas reinhardtii flagellar mutants, ida5 and ida6, that lack a newly identified heavy chain of the inner dynein arm. *Cell Struct. Funct.* **18,** 371–377 (1993).
109. Kamiya, R., Kurimoto, E. & Muto, E. Two types of Chlamydomonas flagellar mutants missing different components of inner-arm dynein. *J. Cell Biol.* **112,** 441–447 (1991).
110. Piperno, G., Mead, K. & Shestak, W. The inner dynein arms I2 interact with a 'dynein regulatory complex' in Chlamydomonas flagella. *J. Cell Biol.* **118,** 1455–1463 (1992).
111. Wirschell, M. *et al.* The nexin-dynein regulatory complex subunit DRC1 is essential for motile cilia function in algae and humans. *Nat. Genet.* **45,** 262–268 (2013).
112. Horani, A. *et al.* CCDC65 mutation causes primary ciliary dyskinesia with normal ultrastructure and hyperkinetic cilia. *PLoS ONE* **8,** e72299 (2013).
113. Rupp, G. & Porter, M. E. A subunit of the dynein regulatory complex in Chlamydomonas is a homologue of a growth arrest-specific gene product. *J. Cell Biol.* **162,** 47–57 (2003).

114. Jeanson, L. *et al.* Mutations in GAS8, a Gene Encoding a Nexin-Dynein Regulatory Complex Subunit, Cause Primary Ciliary Dyskinesia with Axonemal Disorganization. *Hum. Mutat.* **37,** 776–785 (2016).
115. Merveille, A.-C. *et al.* CCDC39 is required for assembly of inner dynein arms and the dynein regulatory complex and for normal ciliary motility in humans and dogs. *Nat. Genet.* **43,** 72–78 (2011).
116. Becker-Heck, A. *et al.* The coiled-coil domain containing protein CCDC40 is essential for motile cilia function and left-right axis formation. *Nat. Genet.* **43,** 79–84 (2011).
117. El-Gebali, S. *et al.* The Pfam protein families database in 2019. *Nucleic Acids Research* **47,** D427–D432 (2019).